PCCP

Reactivity of Zn^{+}_{aq} in high-temperature water radiolysis

Journal:	*Physical Chemistry Chemical Physics*
Manuscript ID	CP-ART-05-2022-002434.R2
Article Type:	Paper
Date Submitted by the Author:	03-Aug-2022
Complete List of Authors:	Lisouskaya, Aliaksandra; University of Notre Dame, Radiation Laboratory Markad , Uddhav ; University of Notre Dame, Radiation Laboratory Carmichael, Ian; University of Notre Dame, Radiation Laboratory and Department of Chemistry & Biochemistry Bartels, David; University of Notre Dame, Radiation Laboratory

ARTICLE

Reactivity of Zn^{+}_{aq} in high-temperature water radiolysis

Aliaksandra Lisouskaya*, Uddhav S. Markad, Ian Carmichael, and David M. Bartels

Received 00th May 2022,
Accepted 00th May 2022

DOI: 10.1039/x0xx00000x

Reactivity of transients involving Zn^{+} in high-temperature water radiolysis has been studied in the temperature range of 25 – 300 °C. The reduced monovalent zinc species were generated from an electron transfer process between the hydrated electron and Zn^{2+} ions using pulse radiolysis. The Zn^{+} species can subsequently be oxidized by the radiolytically-produced oxidizing species: •OH, H_2O_2 and •H. We find that the absorption of monovalent zinc is very sensitive to the pH of the medium. An absorption maximum at 306-311 nm is most pronounced at pH 7 and the signal then decreases in acidic media where the reducing electrons are competitively captured by protons. At pH values higher than 7, hydroxo-forms of Zn^{2+} are created and the maximum of the absorption signal begins to shift to the red spectral region. We find that the optical spectrum of Zn^{+}_{aq} cannot be fully explained in terms of a charge-transfer to solvent (CTTS) process, which was previously proposed. Reaction rates of most of the recombination reactions investigated follow the empirical Arrhenius relationship at temperatures up to 200 °C and have been determined at higher temperatures for the first time. A bimolecular disproportionation reaction of Zn^{+}_{aq} is not observed under the conditions investigated.

Introduction

Over the past few decades, many modifications have been made to the cooling water chemistry in nuclear reactors in order to control the effect of radiation fields on corrosion and, in particular, stress corrosion cracking. Some of these changes include molecular hydrogen addition, zinc addition, and noble metal injection as well as adjustments to pH. Zinc addition into a reactor coolant system was first applied at the Hope Creek Unit, New Jersey for a boiling water reactor in 1987.[1] The original purpose of the zinc addition was to control the buildup of radiation fields from cobalt-60 on out-of-core piping, and since then, plant experience has demonstrated that it can indeed suppress corrosion of materials in reactors. [2-4]

For more than 20 years then, zinc injection (in the form of zinc acetate) has drawn considerable attention in the nuclear industry from these first efforts to mitigate Co-60 deposition in Boiling Water Nuclear Reactors.[5, 6] Zn^{2+} ions have been reported to replace Ni, Fe, and Co ions in spinel-type oxides formed on nickel-based alloys and stainless steels.[7] Zinc-incorporated oxides are thermodynamically more stable and corrosion release rates are significantly mitigated, resulting in a substantial reduction of structural material corrosion. However, continuous zinc injection is necessary to maintain the suppression of corrosion products over the long term.

Despite its successful application, mechanistic details underpinning the roles of Zn^{2+}/Zn^{+} in high-temperature reactor chemistry still remain unclear. We note that, in the presence of Zn^{2+} ions, radiolytically-produced hydrated electrons will generate Zn^{+} transients.[8] This product will subsequently react with the oxidizing species also formed in the system during water radiolysis.

In our previous work, we found that redox reactions of the aqueous $M^{2+/+}$ couples are slow and the rate constants are challenging to determine. This can be explained by a significant change in the local geometry during the course of electron transfer reactions. It is known that divalent zinc ions are coordinated by 6 water molecules[9, 10] while for the monovalent zinc ion, the coordination number was found to be on average equal to 3 or 4 in gas phase measurements.[11] The reduction of Zn^{2+} by the hydrated electron thus involves loss of water molecules from the immediate solvation shell, dramatically reducing the electron transfer reaction rates and probabilities.

For Zn^{2+}, the ion itself is stabilized considerably by its closed-shell characteristic ($3d^{10}$), while upon reduction, the additional electron enters the higher energy level 4s orbital to become Zn^{+} ($3d^{10}4s^{1}$). As a result, the Zn^{2+}/Zn^{+} reduction potential is very negative (less than -1.95V_{SHE}), and only hydrated electrons (E_0 = -2.9V_{SHE}) can easily produce the Zn^{+}.

The present study is aimed to provide a detailed understanding of the radiation chemistry of the Zn^{2+}/Zn^{+} system in high-temperature water. The rate constants and mechanisms of the reactions involved, as well as the extinction coefficient of the reduced Zn^{+}_{aq} species at temperatures up to 300 °C, are determined. This information is of particular importance in developing a more complete and reliable understanding of the effect of zinc ions in water coolant radiolysis and corrosion.

Experimental

Materials

[a] Notre Dame Radiation Laboratory, University of Notre Dame, Notre Dame, IN 46556, USA.

† Footnotes relating to the title and/or authors should appear here.

Electronic Supplementary Information (ESI) available: [details of any supplementary information available should be included here]. See DOI: 10.1039/x0xx00000x

Solutions of $Zn(ClO_4)_2 \cdot 6H_2O$ (Alfa Aesar, 99.997%), $ZnCl_2$ (Sigma-Aldrich, anhydrous, ≥99.999%,) and $ZnSO_4 \cdot 7H_2O$ (Sigma-Aldrich, ≥99.95%) at concentrations of 0.5 – 100 mM saturated with ultrahigh purity argon gas (Airgas) were used throughout the experiment. Methanol (≥99.5%), isopropanol (≥99.5%), sodium formate (99.998%), and *tert*-butanol (anhydrous, ≥99.5%) were purchased from Sigma-Aldrich. All solutions were prepared using ultrapure water from a Serv-A-Pure Co cartridge system (18 MΩ cm resistivity, <10ppb TOC). All other chemicals were obtained from Sigma-Aldrich and used without further purification.

Pulse radiolysis

Pulse radiolysis was carried out using an 8 MeV Linear Accelerator (LINAC) at the Notre Dame Radiation Laboratory, University of Notre Dame. The detection system consisted of a xenon arc lamp light source and a multichannel system capable of recording two-dimensional transient absorption *vs* time traces over a full spectrum as described earlier.[12] For radiation dosimetry, 10 mM KSCN solutions saturated with N_2O were employed; the value $G \times \varepsilon$ of $(SCN)_2^{\bullet -}$ at 475 nm was taken as $(5.28 \pm 0.10) \times 10^{-4}$ m^2 J^{-1}.[13]

The high-temperature kinetics experiments were carried out using two high-pressure syringe pumps (Teledyne Isco Inc), working in constant flow mode, a high-temperature, high-pressure optical cell and temperature-pressure control units.

The solutions from the pumps were mixed at a tee connection, flowed through a preheater coil and then into the optical cell. A 316 stainless steel cell with a 2.5 cm path length and fused silica windows was used for temperatures from 25°C to 200°C. For temperatures above 200°C, a titanium cell with sapphire windows with an optical path of 2.5 cm was employed.

All measurements were carried out using a range of radiation doses from 2.3 to 20 Gy and at least 4 different salt concentrations. Each experiment was reproduced at least three times.

For data fitting the IGOR Pro software package of Wavemetrics, Inc. was employed. Kinetic simulations are evaluated by integration of the appropriate partial differential kinetic equations. The kinetics models were then applied to extract the rate constants of the reactions. Changes in absorbed radiation due to a decrease in water density with increasing temperature was taken into account. The rate constants have also been corrected for ionic strength effects based on the Debye-Brønsted equation.[12] Those rate constants given in the paper are shown at zero ionic strength.

Theoretical calculations

The theoretical calculations were performed using the Gaussian 16, Rev. B.01 program package.[14] Optimized geometries of the resulting radical species were obtained using a range-separated hybrid functional including dispersion corrections (ωB97xD)[15] with a flexible cc-pVTZ basis set.[16] The effect of the solvent was modelled by embedding the radicals in a self-consistent reaction field as implemented in the integral equation formalism of the polarized cavity model. A solvent accessible surface (SAS) was also employed in some calculations to alleviate convergence difficulties[17]. Electronic transition energies and oscillator strengths were calculated by the TD-DFT approach at the optimized geometries initially using the B3LYP functional now with the aug-cc-pVDZ basis set.

Results and Discussion

Kinetic model for the decay of Zn^+_{aq} in water at room temperature

The optical absorption spectrum of Zn^+_{aq} in water at room temperature has been reported previously.[18-23] A similar spectrum was obtained in this study with a λ_{max} at 306-311 nm, as is illustrated in Figure 1.

In the present study, the extinction coefficient $\varepsilon_{310\ nm}$ at room temperature is found to be 11000±600 $M^{-1}cm^{-1}$ formed from zinc sulfate at pH 5.8 and 12510±500 $M^{-1}cm^{-1}$ from zinc chloride salts at pH 5.7 (Fig. 1). These numbers were derived based on $G(e^-)_{aq}$ equal to 2.75 molecules $(100\ eV)^{-1}$, and are corrected for minor competing scavenging of $(e^-)_{aq}$ by acid protons. The numbers are consistent with the values given by Rabani et.al. [23] ($\varepsilon_{310\ nm}$ = 13000 $M^{-1}cm^{-1}$) and by Katsumura et.al[22] ($\varepsilon_{300\ nm}$ = 11500 $M^{-1}cm^{-1}$).

In experiments with 99.995% (metals basis) zinc perchlorate, the extinction coefficient was nominally found to be about 8000±480 $M^{-1}cm^{-1}$ at pH 4 (even with correction for the acid), and increased substantially with temperature. We could not account for the production of 10 mole % acid upon dissolution of this salt, and we ultimately concluded it contains a large impurity that scavenges $(e^-)_{aq}$ very efficiently. It seems likely that the lower extinction coefficients reported by Buxton and Sellers[21] (4700 $M^{-1}cm^{-1}$) and by Baxendale et al. [20] (5200 $M^{-1}cm^{-1}$) were also the result of impurities in the zinc salt used. In all of the works published earlier,[20-23] zinc sulfate salt was used in a concentration range 2 - 20 mM and the pH of the solution during the experiment was not specified.

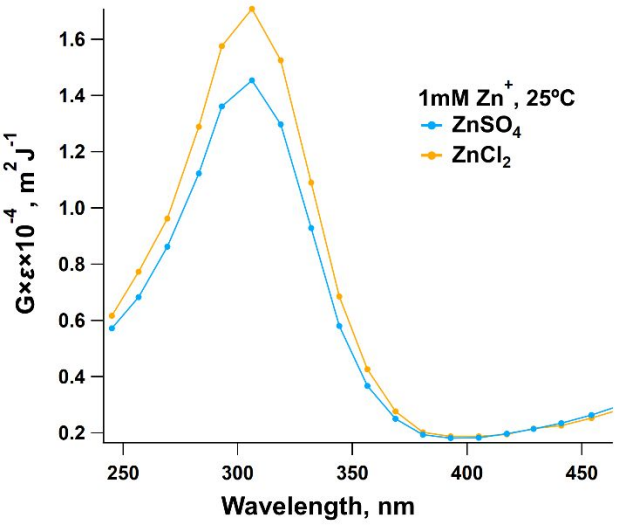

Fig. 1 Transient absorption spectra (G×ε) observed after 9-ns pulse radiolysis in Ar-saturated solutions with 1 mM $ZnSO_4$ (14.7Gy) and $ZnCl_2$ (13.9Gy) at room temperature.

In an Ar-saturated aqueous solution containing Zn^{2+}, formation of the corresponding monovalent zinc ion is complete within a few µs, as is illustrated in Figure 2 for $ZnSO_4$ salt at pH 5.8. The decay kinetics for Zn^{+}_{aq} in $ZnCl_2$ and $Zn(ClO_4)_2$ are shown in Figure S1 (in Supplementary Information). When fitting the kinetic curves, we took into account the pH of the medium, which can change the entire recombination chemistry of the system.

The kinetic model for Zn^{+} decay in the pure water system essentially consists of the reactions (Eq. 1-5) presented in Table 1. First, hydrated electrons will be readily scavenged by Zn^{2+}, generating the corresponding Zn^{+} species (Eq. 1) within 2-3 microseconds after the pulse. The monovalent zinc ions are then consumed in second-order recombination, first reacting mainly with the OH radical (Eq. 2), then also in the reaction with hydrogen peroxide (Eq. 3) and H atom (Eq. 4). According to Rabani, et al, [23] Zn^{+} can also undergo disproportionation with itself and our fitting made use of their rate constant(Eq. 5). The rate constants for water radiolysis reactions (Eq. 6-13) were taken from the review by Elliot and Bartels.[24]

The (averaged) rate constants for reactions (Eq. 1-4) obtained by fitting the data from the pulse radiolysis of $ZnSO_4$ and $ZnCl_2$ at room temperature are presented in Table 1.

The room temperature rate constants for the reactions of Zn^{+}_{aq} with radiolytic oxidizing species have been determined previously.[21, 23, 25] The present rate constant for $^{\bullet}OH$ is in agreement with the literature value, reported by Buxton[21] (Table 1). The rate constant for the H_2O_2 reaction is close to the value measured in earlier works by Meyerstein and Mulac, Buxton and Sellers, and Rabani, et al. [21, 23, 25] Our data was not sensitive to the reaction with $^{\bullet}H$ (Eq. 4) because the second order decay is dominated by the reaction of Zn^{+}_{aq} with $^{\bullet}OH$ (Eq. 2). We used the rate constant similar to $k = 1 \times 10^9$ $M^{-1}s^{-1}$, reported by Rabani, et al[23] in H_2-saturated solutions.

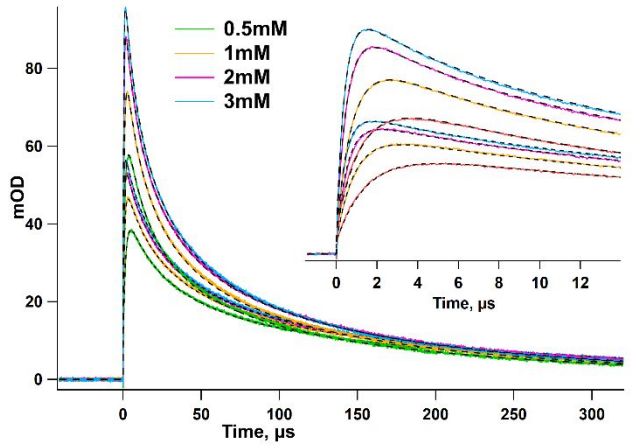

Fig. 2 Decay kinetics of Zn^{+}_{aq} at 306nm formed on 4ns and 9ns-pulse radiolysis (7.7Gy and 14.7Gy) of 0.5-3 mM $ZnSO_4$ solutions saturated with Ar. The fit curves are shown in black.

Table 1. Rate constants of the reactions listed (1-13) applied in the kinetics model for Zn^{+}_{aq} decay at room temperature at zero ionic strength

№	Reaction	Rate Constant, $k \times 10^9$ $M^{-1}s^{-1}$
		current data
1	$(e^-)_{aq} + Zn^{2+} \rightarrow Zn^{+}$	1.3±0.06 (this work); 1.6 [8];1.8[22];1.5 [20, 26, 27]; 0.95[23] ; 1.0[28]
2	$Zn^{+} + {}^{\bullet}OH \rightarrow Zn^{2+} + OH^-$	11.8±0.6 (this work); 20 [21] ;15[29]
3	$Zn^{+} + H_2O_2 \rightarrow Zn^{2+} + {}^{\bullet}OH + OH^-$	2.2±0.05 (this work); 2.4 [23] ; 2.3[30]; 1.8[25]
4	$Zn^{+} + {}^{\bullet}H\ (+H^+) \rightarrow Zn^{2+} + H_2$	1.0[23]
5	$Zn^{+} + Zn^{+} \rightarrow Zn^{0} + Zn^{2+}$	0.35[23]
6	$(e^-)_{aq} + (e^-)_{aq} + 2H_2O \rightarrow H_2 + 2OH^-$	7.3[24]
7	$(e^-)_{aq} + {}^{\bullet}OH \rightarrow OH^-$	35.6[24]
8	$(e^-)_{aq} + {}^{\bullet}H + H_2O \rightarrow H_2 + OH^-$	27.6[24]
9	$(e^-)_{aq} + H^+ \rightarrow {}^{\bullet}H$	21.0 [24].
10	$(e^-)_{aq} + H_2O_2 \rightarrow {}^{\bullet}OH + OH^-$	13.6[24]
11	$^{\bullet}OH + {}^{\bullet}OH \rightarrow H_2O_2$	4.8[24]
12	$^{\bullet}H + {}^{\bullet}OH \rightarrow H_2O$	10.9[24]
13	$^{\bullet}H + {}^{\bullet}H \rightarrow H_2$	5.13[24]

It is expected that the disproportionation reaction (5) is relatively slow. Rabani et al. [23] have reported the rate constant at room temperature for this reaction in the Zn^{+}_{aq} system to be 3.5×10^8 $M^{-1}s^{-1}$. Moreover, in a number of previous works under similar conditions at room temperature, a greyish precipitate has been detected and identified as zinc metal.[21, 31] When fitting our data, we found that the disproportionation reaction had no effect on the fit and we kept the value of 3.5×10^8 $M^{-1}s^{-1}$ (Table 1). At the same time, after irradiation of the solutions, we did not see any signs of metal zinc precipitation.

Effect of pH on the Zn^{+}_{aq} spectrum

Divalent zinc ions in aqueous solutions are known to form stable zinc oxides in the pH range of 8–12.[32] Above pH 7, metal hydrolysis generates $Zn(OH)^{+}$. At pH 9-11, the predominant species is insoluble $Zn(OH)_2$. Above pH 12.5, zinc hydroxy complexes such as $Zn(OH)_3^-$ and $Zn(OH)_4^{2-}$ are more stable.

We probed the influence of the pH on the absorption spectrum of the monovalent zinc ion formed during pulse radiolysis of 1 mM $Zn(ClO_4)_2$ solutions saturated with Ar (Figure3).

It should be noted that the pH of the solution changes with concentration (Figure S2 in Supplementary Information) due to acid from perchlorate salt. When fitting the kinetic curves, we took into account the pH of the medium. As can be seen from the spectrum in Figure 3, the maximum G×ε value is found at pH 7 and the signal then decreases upon transition to a more acidic medium. In the acidic environment, electrons will be captured by protons to give H atoms (Eq. 9) in competition with the scavenging by Zn^{2+}.

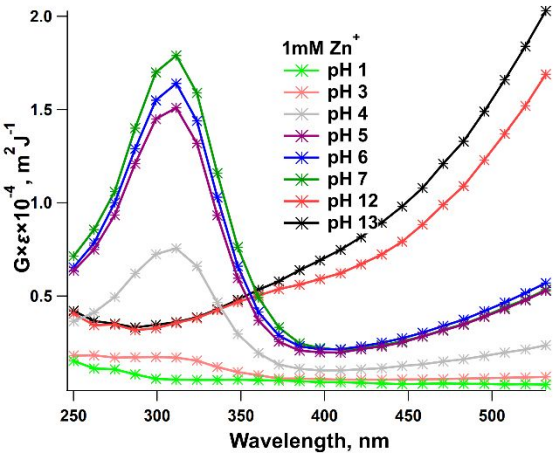

Fig. 3 Transient absorption spectra observed 2 μs after 10-ns pulse radiolysis (10 Gy) in Ar-saturated 1 mM $Zn(ClO_4)_2$ solutions at different pH at room temperature.

It is obvious from the lack of signal at low pH that hydrogen atoms do not readily reduce Zn^{2+}. Indeed, Katsumura and coworkers[22] previously attempted to observe a reaction of H• atoms (E^0 = −2.31V vs SHE) with Zn^{2+} in strong acid but also found no reaction.

At pH higher than 7, the maximum of the UV signal begins to shift toward the red, reaching 360 nm at pH 12. In strong alkali, H atoms are converted to hydrated electrons (•H ⇌ $(e^-)_{aq}$ + H^+, pKa= 9.6 at 25°C)[33, 34] and OH radicals deprotonate (•OH ⇌ $O^{\bullet-}$ + H^+, pKa= 11.9)[35]. As can be seen from figure 3, upon transition to more alkaline solutions, the absorption due to hydrated electrons in the visible region increases.

In previous studies, [18, 22, 36] it was shown that the reactivity of Zn^{2+} with the hydrated electron also depends on pH in alkaline solutions since Zn^{2+} exists in various hydroxo-forms ($Zn(OH)_4^{2-}$ and $Zn(OH)_3^-$). The rate constant of reaction with the electron (Eq. 1) decreases with an increase in hydroxide concentration from 1 to 5 M from roughly 10^7 to 10^6 $M^{-1}s^{-1}$. In the work of Pikaev et al.[18], a redshift in the absorption maximum of the spectrum in strongly alkaline solutions was also observed.

It can be seen from the above data that the absorption of divalent zinc is very sensitive to the pH of the medium. Small changes in pH above 7 will significantly affect the extinction coefficient of Zn^+.

Decay of Zn^+_{aq} in the presence of scavengers of •OH and •H

It is expected that the disproportionation reaction (Eq. 5) is relatively slow compared to the reactions of Zn^+_{aq} with the active oxidizing species (Eq. 3-5) (Table 1). However, in the presence of •OH and •H scavengers, the disproportionation reaction might be expected to be observable. For this reason, 0.1 M methanol, *tert*-butanol and formate were added into the system with zinc to scavenge both •OH and •H.

Added methanol and *tert*-butanol react with •OH radicals and H atoms forming carbon-centered radicals, the hydroxymethyl radical ($•CH_2OH$) and the 2-hydroxy-2,2-dimethylethyl radical ($•CH_2C(CH_3)_2OH$), as illustrated for methanol in equations (14-15). The rate constants at room temperature for the •OH reactions are 8-9.7 × 10^8 and 6 × 10^8 $M^{-1}s^{-1}$ for methanol and *tert*-butanol, respectively.[37, 38] The rate constants for reaction with the H atom are much slower, 3 × 10^6 for methanol and 1 × 10^5 $M^{-1}s^{-1}$ for *tert*-butanol. [38]

$$CH_3OH + •OH \rightarrow •CH_2OH + H_2O \quad (14)$$

$$CH_3OH + H \rightarrow •CH_2OH + H_2 \quad (15)$$

Added formate will react with •OH (Eq. 14) and •H (Eq. 15) forming the $CO_2^{•-}$ radical anion with rate constants 3.2 × 10^9 and 2.1 × 10^8 $M^{-1}s^{-1}$,[39, 40] respectively. Both the carbon-centered radicals and $CO_2^{•-}$ in (Eq. 14-15) will undergo further recombination reactions, for example (Eq. 16).

$$•CH_2OH + •CH_2OH \rightarrow \text{products} \quad (16)$$

These scavenging processes should also eliminate the majority of H_2O_2 otherwise coming from the recombination of •OH radicals (11) (Table 1).

Decay kinetics with the addition of methanol, *tert*-butanol and formate over a 50-microsecond time period after the electron pulse are presented in Figure 4. To fit the data we used the kinetic model from Table 1, with additional reactions involving •OH and •H scavengers (14-16). In systems with the addition of •OH and •H scavengers, the decay kinetics of Zn^+ should be mainly due to the reaction with the carbon-centered alcohol radicals and the $CO_2^{•-}$ radical anion.

Rabani et al.[23] proposed the following mechanism for the Zn^+ oxidation to Zn^{2+} with alcohol radicals (Eq. 17).

$$•CH_2OH + Zn^+ + H^+ \rightarrow Zn^{2+} + CH_3OH \quad (17)$$

They reported the rate constants for the reaction with methanol and *tert*-butanol to be equal to 2.5 × 10^9 $M^{-1}s^{-1}$ and 1.3 × 10^9 $M^{-1}s^{-1}$, respectively. They also suggested that this process (Eq. 17) may include the formation of transient species of monovalent zinc with the alcohol radical, such as $(ZnCH_2OH)^+$. Similar adduct formation was identified in the systems containing methanol with Ni^+ by Kelm et al.[41]

The reaction rate constants of Zn^+ with methanol and *tert*-butanol radicals as extracted from data fitting are 2.4 × 10^9 and 1.5 × 10^9 $M^{-1}s^{-1}$, respectively These values are similar to those previously published by Rabani, et al.[23] It is noticeable that in the systems with formate the signal intensity is 2 times higher (Figure 4). In this case, the pH of the medium will be about 7, which corresponds to the maximum intensity of the zinc signal as shown in Figure 3.

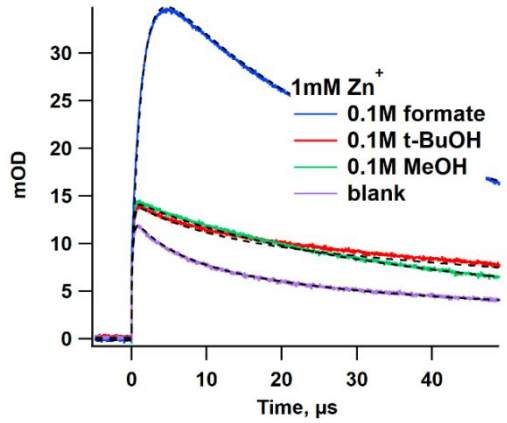

Fig. 4 Decay kinetics of Zn^{+}_{aq} at 311nm formed on 8ns (18.5Gy) pulse radiolysis of 1 mM $Zn(ClO_4)_2$ solutions with 0.1 M methanol, *tert*-butanol and formate, saturated with Ar. The fit curves are shown in black.

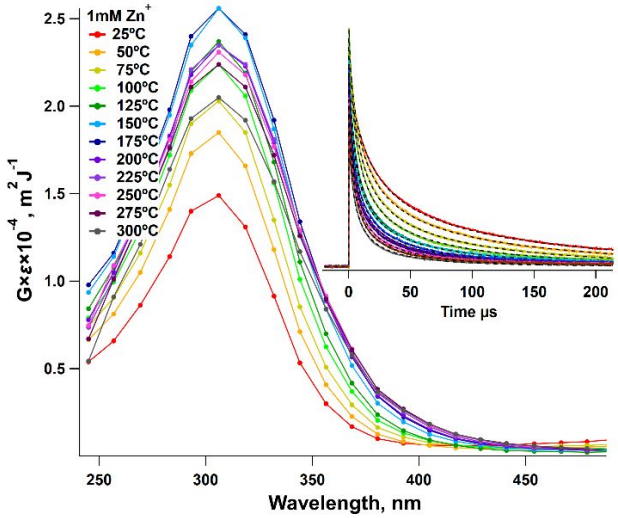

Fig. 5 Transient absorption spectra and decay kinetics (insert) at 306 nm observed after 9-ns pulse radiolysis in Ar-saturated solutions with 1 mM $ZnSO_4$ at a temperature range from 25 to 300 °C (~17Gy). The fit curves are shown in black.

The alcohol solutions were run with pH=4. In previous work Rabani et. al.,[23] found no evidence that $CO_2^{\bullet-}$ radicals (E^0=-1.9V vs SHE)[42, 43] can reduce the divalent zinc ions. Katsumura et al.,[22] demonstrated that neither the 2-hydroxy-2,2-dimethylethyl radical nor the 1-hydroxyethyl radical reduce Zn^{2+}. When fitting our data, we confirmed that neither $CO_2^{\bullet-}$ radical nor alcohol radicals can reduce divalent zinc ions.

Our estimate of the rate for the reaction of Zn^{+} with $CO_2^{\bullet-}$ radicals is 5.6×10^9 $M^{-1}s^{-1}$, corrected to zero ionic strength.

From the data obtained it follows that Zn^{+}_{aq} rapidly reacts with radicals formed from OH and H radical scavengers, and the disproportionation reaction does not contribute to the decay kinetics.

The disproportionation reaction is energetically unfavorable in the gas phase, but in an aqueous medium, it could occur. To confirm this we performed several quantum chemical calculations on the energetics of the disproportionation reaction of monovalent zinc in water. The model system employed a 24 water molecule cluster optimized on its own (wb97xD/pc-1) [15, 44, 45], then containing either Zn^{+} or Zn^{2+} ions, in addition to an isolated zinc atom. The surrounding solvent was in turn modeled by the self-consistent reaction field approach[46]. From the calculated energies, we have established that this reaction is exothermic with ΔG ~220 kJ mol^{-1}, and so is energetically favorable. But to get a complete picture of the process, we would, of course, need to assess how large the barrier is, which can greatly slow down the reaction. This would involve detailing the actual mechanism(s) of the disproportionation reaction, a task which we have not here attempted.

Kinetic model for the decay of Zn^{+}_{aq} in water at high temperatures

The reactions of aqueous Zn(II) ions under irradiation up to high temperatures have been measured here for the first time. Figure 5 illustrates transient absorption spectra expressed in G×ε values and the decay kinetics (inserts) of monovalent zinc formed in $ZnSO_4$ at temperatures up to 300 °C.

Transient absorption spectra and decay kinetics for Zn^{+}_{aq} formed in $Zn(ClO_4)_2$ and $ZnCl_2$ are shown in Figure S3 in the Supporting Information. The second-order decay of the monovalent zinc ions is dominated by the reaction with the $^{\bullet}OH$ radical. Table S1 includes kinetic information for $ZnSO_4$ and $ZnCl_2$ recovered from the experimental data by fitting the kinetic curves. In experiments with zinc perchlorate, the apparent rate constant of Zn^{2+} with $(e^-)_{aq}$ was much higher at high temperatures because it contains an impurity that scavenges $(e^-)_{aq}$ very efficiently. The product of this reaction must have a similar spectrum to that of Zn+, because the initial absorbance is nearly the same.

It can be seen from the tabulated data that with an increase in temperature, the reaction rates increase. The rate constants for reactions (Eq. 6-13) at high temperatures were taken from the review of Elliot and Bartels.[24] The Arrhenius plots of the reactions of Zn^{+}_{aq} are given in Figure 6. The activation energies (E_a) and Arrhenius pre-factors (A) from these plots are summarized in Table 2.

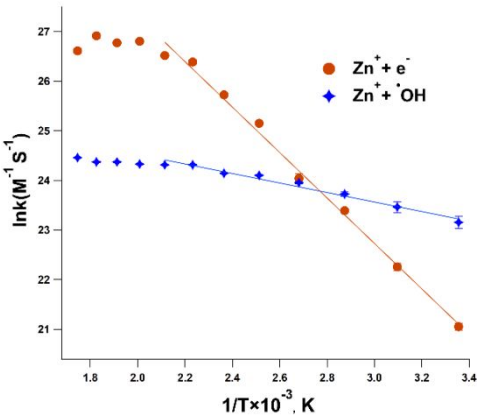

Fig. 6 Arrhenius plots of the rate constants of Zn^{+}_{aq} for reactions (1-2) in the temperature range of 25 – 300 °C.

Table 2. Parameters of the main reactions (1-4) applied in the kinetics model for Zn^{+}_{aq} decay at temperatures up to 300ºC

№	Reaction	E_a, kJ/mol	A, $M^{-1}s^{-1}$
1	$(e^{-})_{aq} + Zn^{2+} \rightarrow Zn^{+}$	38.0±1.0	6.4×10^{15}
2	$Zn^{+} + {}^{\bullet}OH \rightarrow Zn^{2+} + OH^{-}$	8.5±1.5	2.9×10^{11}
3	$Zn^{+} + H_2O_2 \rightarrow Zn^{2+} + {}^{\bullet}OH + OH^{-}$	7.3±1.6	4.4×10^{10}

The parameters obtained for the reaction of zinc with hydrated electrons up to 200 °C are consistent with the values previously published.[8] The reaction rate becomes nearly constant above 200ºC, which was not detected previously using the perchlorate salt.

Reaction of Zn^{+}_{aq} with $^{\bullet}OH$ (Eq. 2) also exhibits Arrhenius behavior up to 200 °C and then reaches a plateau (Figure 6). Even in acidic pH 4 solutions with substantial H concentration, it proved impossible to cleanly separate any rate constant for H reaction with Zn^{+}_{aq} from the second order decay dominated by $^{\bullet}OH$. The H_2O_2 reaction was separable in global fitting of multiple dose curves due to its production from $^{\bullet}OH$ recombination.

The reaction between Zn^{+}_{aq} and $^{\bullet}OH$ is likely to occur via two consecutive steps. First, Zn^{+}_{aq} forms an intermediate with $^{\bullet}OH$ generating an intermediate $ZnOH^{+}$. Given that the Zn^{+} is only coordinated by 3 or 4 water molecules this should be easily accomplished. Second, $ZnOH^{+}$ accepts a proton from water (and coordinates another water molecule) to produce the final product, Zn^{2+}_{aq}. A similar mechanism has been proposed previously for the reaction of Ni^{+}_{aq} with the OH radical.[21]

The reaction of $^{\bullet}H$ with Zn^{+}_{aq} can be electron transfer or H atom addition to monovalent zinc ion similar to the reaction with $^{\bullet}OH$. The redox potential of the $^{\bullet}H/H^{-}$ couple has been estimated to be 0.05V *vs* SHE.[47] Monovalent zinc ions should reduce $^{\bullet}H$ rapidly according to reaction (Eq. 4) (Table 1), though the rate must remain significantly slower than that of reaction 2.

For the reactions with H_2O_2, Buxton *et al*.[30] have shown that most of the H_2O_2 reactions with $M^{+}_{(aq)}$ (Cd^{+}_{aq}, Co^{+}_{aq}, and Zn^{+}_{aq}) occur through electron transfer. According to Buxton *et al*., [30] the activation energy for the reaction of Zn^{+} with H_2O_2 in a narrow temperature range was 10.5 kJ/mol. The activation energy for the reaction of H_2O_2 with Zn^{+}_{aq} in the present study appears to be about 7.3 kJ/mol (Table 2), which corresponds to the data obtained earlier within the stated error bars. [30]

Transitions in the Zn^{+}_{aq} spectrum

The electronic absorption of the Zn^{+} species were originally assigned to charge-transfer-to-solvent (CTTS) transition spectra based on experimental data where monovalent metal ions Cd^{+}, Zn^{+}, Co^{+}, and Ni^{+} produce hydrated electrons when photolyzed with UV light. [19]

Such CTTS transitions represent the simplest possible charge transfer reaction (seen, for example, in halides) when electron transfer from an atomic ion to a cavity in the surrounding solvent involves only electronic degrees of freedom.[48] The normal temperature-dependent characteristic of CTTS spectra is that the band shifts toward the red with an increase in temperature.[49] Other characteristics of CTTS transitions are blue shifts with a salt addition and extreme solvent sensitivity.

The temperature dependence of these metal cation spectra has not been previously reported. The spectrum of Zn^{+} measured up to 300 °C does not change shape (Figures 5, S3).

We tested the effect of a solvent on the behavior of the spectrum of Zn^{+} at room temperature. The change of the solvent could completely alter the events that occur during radiolysis. We compared the spectrum of zinc formed in methanol and isopropanol solutions (Figure S4). In these systems, the peak is shifted to the short-wavelength region (blue shift). The reaction rates between solvated electrons and zinc ions proceeds 10-20 times faster than in water. This may be due to the formation of ($e^{-}_{solv}Zn^{2+}$) transients in alcohol solutions as was proposed by Hickel. [50] Therefore, the shift of the Zn^{+} peak in the solvent can also be caused by the formation ($e^{-}_{solv}Zn^{2+}$) transients, and nothing can be concluded regarding the nature of the transition in water.

It is apparent that many of the expected CTTS characteristics are not present in the monovalent zinc spectrum, which most likely means that the previous assignment of CTTS for this transition is incorrect. In anion CTTS systems, the primary stabilization of the incipient solvated electron comes from the "reaction potential" well induced by the anion itself. It is difficult to imagine how any such effect can be obtained in cation systems. If solvated electrons are indeed produced in this excitation, it may be from autoionization following an allowed 4s->5p transition.

TD-DFT calculations of excitation of Zn^{+}_{aq} species

Details of the hydration and water exchange mechanism of Zn^{2+} have been studied using density functional theory calculations with a variety of different basis sets. [51]

The character and degree of the inner-sphere reorganization during electroreduction of aqua, aquahydroxy, and hydroxyl complexes of Zn^{2+} has been studied previously using B3LYP, PM3 and MNDO computational methods.[52]

Using the TD-DFT approach, we calculated the absorption spectrum of the monovalent zinc ion coordinated by 3 water molecules and/or hydroxide ions. The optimized quantum chemical geometries and structures of the main species are presented in Table S2, and Figure 7 shows their calculated absorption spectra. The computed absorption spectrum of the three-water complex has an intense signal, centered at about 360 nm (Fig. 7) which appears to be a localized Zn^{+}-ion-centered transition. As the water molecules are replaced by consecutive hydride ion substitutions, it can be seen that the spectrum shifts to the red region (Figure 7). These results are consistent with the behavior of the measured experimental spectra. In calculations with 3 and 4 water molecules, the fourth water was observed to go into a second shell. Thus, gas phase measurement[11] agrees with our limited simulations of coordination number in solution.

We also performed calculations of Zn^{+}– water clusters with up to 24 water molecules. For the smaller clusters, the zinc ion is located on the surface of the cluster and the predicted

transitions are similarly centered on the zinc cation. However, in the largest clusters the ion is centrally located and, while the lowest energy transition is clearly metal centered, some states reached by higher-energy transitions seem to have a metal to solvent component (shown in Figure S5). It is not hard to conceive that any of these states can be coupled to adjacent "solvent cavity" states to form hydrated electrons. The photochemical effect is the same as for traditional CTTS transitions of anions, but here might be better termed autoionization of the excited states.

Calculations described above for the s-p transition of Zn^+ in the gas phase show a band at 202 nm for the triply degenerate s-p transition, but when the ion is surrounded by an unstructured polarizable continuum, the transition shifts almost 60 nm to the red. It is important to note that when we add an explicit water molecule the s-p absorption splits into three bands of roughly equal intensity and redshifts by around 40 nm. The more explicit water molecules are added, the further these band will shift to the red.

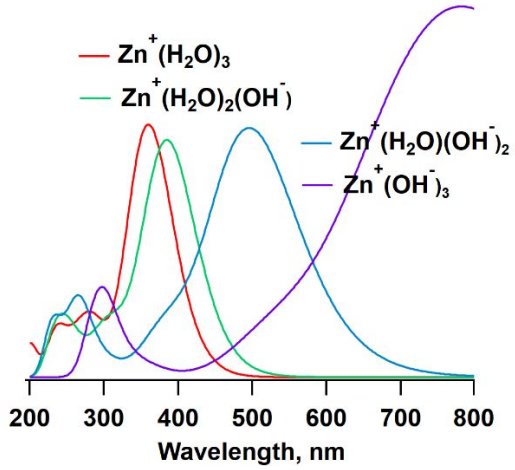

Fig. 7 TD-DFT calculated absorption spectra of Zn^+_{aq} coordinated by water molecules and hydroxyl ions.

Conclusions

This high-temperature pulse radiolysis study has provided new information involving the oxidation-reduction reactions of the monovalent transition-metal zinc ions, Zn^+_{aq}, in pure water.

This investigation of the reactions of Zn^+_{aq} has given insight into not only the optical spectra of the species involved but also kinetic and thermodynamic information on the reacting systems. It appears that at temperatures up to 300 °C, the spectrum of Zn^+_{aq} is well-preserved in terms of both shape and λ_{max}. The spectral characteristics at high temperature of the monovalent zinc ions, therefore, cannot be fully explained in terms of CTTS as has been previously claimed. At the longest wavelengths is well described by metal centered s-p like transitions, though we did note certain Zn^+_{aq} clusters in which a CTTS contribution is present at higher energies in the predicted spectrum. We have demonstrated that the maximum absorption of Zn^+_{aq} occurs at neutral pH. This can be explained by the number of protons in the system, which compete in the reaction with electrons, as well as the formation of Zn^+_{aq} hydroxo-forms in an alkaline medium.

The kinetics data have demonstrated that Zn^+_{aq} ions are reactive toward the radiolytically produced oxidizing species from water, particularly the •OH radical. The reactions investigated follow an empirical Arrhenius relationship at temperatures up to 200 °C and then tend to reach a plateau value. Our data showed that disproportionation of Zn^+_{aq} does not affect the kinetics under the conditions investigated.

Conflicts of interest

There are no conflicts to declare.

Acknowledgements

The pulse radiolysis experiments and theoretical calculations at the Notre Dame Radiation Laboratory were supported by the U.S. Department of Energy, Office of Science, Office of Basic Energy Sciences under award number DE-FC02-04ER15533.

This is document number NDRL-5349 from the Notre Dame Radiation Laboratory.

Snapshots from MD simulations of Zn2+ in water were kindly provided by Gregory Schenter from Pacific Northwest National Laboratory, WA.

Quantum chemical calculations were performed on machines in the Center for Research Computing at the University of Notre Dame.

Notes and references

Supporting Information. Structures, optimized quantum mechanical geometries, additional spectroscopic and kinetic information.

REFERENCES

1. C. J. Wood, *Nuclear Engineering International*, 1991, **36**, 39-40.
2. S. E. Ziemniak and M. Hanson, *Corrosion Science*, 2006, **48**, 2525-2546.
3. X. Liu, X. Wu and E.-H. Han, *Corrosion Science*, 2012, **65**, 136-144.
4. J. Huang, X. Liu, E.-H. Han and X. Wu, *Corrosion Science*, 2011, **53**, 3254-3261.
5. W. J. Marble, R. L. Cowan and C. J. Wood, in *Water Chemistry of Nuclear Reactor Systems*, Thomas Telford Publishing, 1986, pp. 113-119.
6. C. C. Lin, *Progress in Nuclear Energy*, 2009, **51**, 207-224.
7. V. Cantatore, C. Geers, J. Chen and I. Panas, *Journal of Nuclear Materials*, 2020, **540**, 152361-152361.
8. K. Kanjana, B. Courtin, A. MacConnell and D. M. Bartels, *Journal of Physical Chemistry A*, 2015, **119**, 11094-11104.
9. C. Jana, G. Ohanessian and C. Clavaguéra, *Theoretical Chemistry Accounts*, 2016, **135**, 135-141.
10. Y. Ikushima, N. Saito and M. Arai, *The Journal of Physical Chemistry B*, 1998, **102**, 3029-3035.
11. B. Bandyopadhyay, K. N. Reishus and M. A. Duncan, *The Journal of Physical Chemistry A*, 2013, **117**, 7794-7803.
12. A. Lisovskaya, K. Kanjana and D. M. Bartels, *Physical Chemistry Chemical Physics*, 2020, **22**, 19046-19058.

13. G. V. Buxton and C. R. Stuart, *Journal of the Chemical Society, Faraday Transactions*, 1995, **91**, 279-279.
14. M. J. Frisch, G. W. Trucks, H. B. Schlegel, G. E. Scuseria, M. A. Robb, J. R. Cheeseman, G. Scalmani, V. Barone, G. A. Petersson, H. Nakatsuji, X. Li, M. Caricato, A. V. Marenich, J. Bloino, B. G. Janesko, R. Gomperts, B. Mennucci, H. P. Hratchian, J. V. Ortiz, A. F. Izmaylov, J. L. Sonnenberg, Williams, F. Ding, F. Lipparini, F. Egidi, J. Goings, B. Peng, A. Petrone, T. Henderson, D. Ranasinghe, V. G. Zakrzewski, J. Gao, N. Rega, G. Zheng, W. Liang, M. Hada, M. Ehara, K. Toyota, R. Fukuda, J. Hasegawa, M. Ishida, T. Nakajima, Y. Honda, O. Kitao, H. Nakai, T. Vreven, K. Throssell, J. A. Montgomery Jr., J. E. Peralta, F. Ogliaro, M. J. Bearpark, J. J. Heyd, E. N. Brothers, K. N. Kudin, V. N. Staroverov, T. A. Keith, R. Kobayashi, J. Normand, K. Raghavachari, A. P. Rendell, J. C. Burant, S. S. Iyengar, J. Tomasi, M. Cossi, J. M. Millam, M. Klene, C. Adamo, R. Cammi, J. W. Ochterski, R. L. Martin, K. Morokuma, O. Farkas, J. B. Foresman and D. J. Fox, *Journal*, 2016.
15. J. D. Chai and M. Head-Gordon, *Physical Chemistry Chemical Physics*, 2008, **10**, 6615-6620.
16. T. H. Dunning Jr, *The Journal of chemical physics*, 1989, **90**, 1007-1023.
17. J. Wang, W. Wang, S. Huo, M. Lee and P. A. Kollman, *The Journal of Physical Chemistry B*, 2001, **105**, 5055-5067.
18. A. V. Gogolev, I. E. Makrov and A. K. Pikaev, *High Energy Chemistry*, 1981, **15**, 85-89.
19. N. Basco, S. K. Vidyarthi and D. C. Walker, *Canadian Journal of Chemistry*, 1974, **52**, 343-347.
20. J. H. Baxendale, E. M. Fielden and J. P. Keene, *Proceedings of the Royal Society of London. Series A. Mathematical and Physical Sciences*, 1965, **286**, 320-336.
21. G. V. Buxton and R. M. Sellers, *Journal of the Chemical Society, Faraday Transactions 1: Physical Chemistry in Condensed Phases*, 1975, **71**, 558-558.
22. M. Domae, N. Chitose, Z. Zuo and Y. Katsumura, *Radiation Physics and Chemistry*, 1999, **56**, 315-322.
23. J. Rabani, W. A. Mulac and M. S. Matheson, *Journal of Physical Chemistry*, 1977, **81**, 99-104.
24. A. J. Elliot and D. M. Bartels, *Atomic Energy of Canada Limited Report*, 2009, 153-127160.
25. D. Meyerstein and W. A. Mulac, *Journal of Physical Chemistry*, 1968, **72**, 784-788.
26. A. Blum and L. I. Grossweiner, *Photochemistry and Photobiology*, 1982, **36**, 617-622.
27. D. Meyerstein and W. A. Mulac, *Journal of Physical Chemistry*, 1969, **73**, 1091-1095.
28. F. Barat, L. Gilles, B. Hickel and B. Lesigne, *The Journal of Physical Chemistry*, 1973, **77**, 1711-1715.
29. J. H. Baxendale, J. P. Keene and D. A. Stott, *ChemComm*, 1966, **20**, 715-716.
30. G. V. Buxton, R. M. Sellers and D. R. McCracken, *Journal of the Chemical Society, Faraday Transactions 1: Physical Chemistry in Condensed Phases*, 1976, **72**, 1464-1464.
31. J. H. Baxendale and R. S. Dixon, *Zeitschrift für Physikalische Chemie*, 1964, **43**, 161-176.
32. S. Thomas, N. Birbilis, M. S. Venkatraman and I. S. Cole, *Corrosion Science*, 2013, **69**, 11-22.
33. E. J. Hart, S. Gordon and E. Fielden, *The Journal of Physical Chemistry*, 1966, **70**, 150-156.
34. H. Shiraishi, G. R. Sunaryo and K. Ishigure, *The Journal of Physical Chemistry*, 1994, **98**, 5164-5173.
35. J. Rabani and M. Matheson, *The Journal of Physical Chemistry*, 1966, **70**, 761-769.
36. M. Anbar and E. J. Hart, *Journal of Physical Chemistry*, 1965, **69**, 973-977.
37. N. Motohashi and Y. Saito, *Chemical and pharmaceutical bulletin*, 1993, **41**, 1842-1845.
38. W. Tsang, *Journal of Physical and Chemical Reference Data*, 1988, **17**, 887-951.
39. G. V. Buxton, C. L. Greenstock, W. P. Helman and A. B. Ross, *Journal of Physical and Chemical Reference Data*, 1988, **17**, 513-886.
40. M. Chin and P. Wine, in *Aquatic and Surface Photochemistry*, CRC press, 2018, pp. 85-96.
41. M. Kelm, J. Lilie, A. Henglein and E. Janata, *Journal of Physical Chemistry*, 1974, **78**, 882-887.
42. P. S. Rao and E. Hayon, *Journal of the American Chemical Society*, 1974, **96**, 1287-1294.
43. H. A. Schwarz and R. W. Dodson, *The Journal of Physical Chemistry*, 2002, **93**, 409-414.
44. F. Jensen, *The Journal of Chemical Physics*, 2001, **115**, 9113-9125.
45. F. Jensen, *The Journal of Chemical Physics*, 2002, **116**, 7372-7379.
46. J. Tomasi, B. Mennucci and R. Cammi, *Chemical Reviews*, 2005, **105**, 2999-3094.
47. P. Toffel and A. Henglein, *Faraday Discussions of the Chemical Society*, 1977, **63**, 124-133.
48. M. J. Blandamer and M. F. Fox, *Chemical Reviews*, 1970, **70**, 59-93.
49. T. W. Marin, I. Janik and D. M. Bartels, *Physical Chemistry Chemical Physics*, 2019, **21**, 24419-24428.
50. B. Hickel, *The Journal of Physical Chemistry*, 1978, **82**, 1005-1010.
51. M. Hartmann, T. Clark and R. van Eldik, *Journal of the American Chemical Society*, 1997, **119**, 7843-7850.
52. R. R. Nazmutdinov, M. S. Shapnik, E. E. Starodubets and T. P. Petrova, *Russian Journal of Electrochemistry*, 2002, **38**, 1339-1345.